ELSEVIER

Tectonophysics 351 (2002) 315–329

TECTONOPHYSICS

www.elsevier.com/locate/tecto

The influence of matrix rheology and vorticity on fabric development of populations of rigid objects during plane strain deformation

Sandra Piazolo [a,b,*], P.D. Bons [a,1], C.W. Passchier [a,1]

[a] *Tektonophysik, Institut für Geowissenschaften, Johannes Gutenberg Universität, Becherweg 21, D-55099 Mainz, Germany*
[b] *Department of Geological Mapping, Geological Survey of Denmark and Greenland, Thoravej 8, DK-2400 Copenhagen NV, Denmark*

Received 18 January 2001; accepted 18 April 2002

Abstract

The influence of vorticity and rheology of matrix material on the development of shape-preferred orientation (SPO) of populations of rigid objects was experimentally studied. Experiments in plane strain monoclinic flow were performed to model the fabric development of two populations of rectangular rigid objects with object aspect ratios (R_{ob}) 2 and 3. The density of the rigid object populations was 14% of the total area. Objects were dispersed in a Newtonian and a non-Newtonian, power law matrix material with a power law exponent n of 1.2. The kinematic vorticity number (W_n) of the plane strain monoclinic flow was 1, 0.8 and 0.6 with finite simple shear strain of 4.6, 3.0 and 0.9, respectively. In experiments with R_{ob}=3, the SPO is strongly influenced by W_n and the material properties of the matrix. Deformation of a power law matrix material and low W_n resulted in a stronger SPO than deformation of a linear viscous matrix and high W_n. Strain localization coupled with particle interaction plays a significant role in the development of a shape-preferred orientation. High strain simple shear zones separate trains of rigid objects that are surrounded by low strain zones with W_n lower than the bulk W_n. In fabrics involving populations of objects with R_{ob}=2, rheology of the matrix materials does not systematically influence the intensity of the SPO.

Keywords: Analogue modelling; Shape-preferred orientation; General flow; Strain localization; Power law flow

1. Introduction

Rigid inclusions and matrix systems form an important class of structures that are used for structural and kinematic analysis. One of these structures is the shape-preferred orientation (SPO) of a population of elongated rigid objects. Examples are populations of mm-scale feldspar laths dispersed in granitic melt or crystal mush (e.g. Bouchéz, 1997; Vernon, 2000), amphiboles in a fine-grained feldspar-mica mylonite (e.g. Ildefonse et al., 1990), garnet, plagioclase, sillimanite in a high temperature mylonite (Pennacchioni et al., 2001) and mica in a fine-grained slate (e.g. Tullis and Wood, 1975). Data on finite strain and type of flow can potentially be derived from characteristics of the shape-preferred orientation (e.g. Rees, 1968,

* Corresponding author. Department of Geological Mapping, Geological Survey of Denmark and Greenland, Thoravej 8, DK-2400 Copenhagen NV, Denmark. Tel.: +45-3814-2271; fax: +45-3814-2050.

E-mail address: spi@geus.dk (S. Piazolo).

[1] Tel.: +49-6131-3924527; fax: +49-6131-3923863.

0040-1951/02/$ - see front matter
PII: S0040-1951(02)00220-2

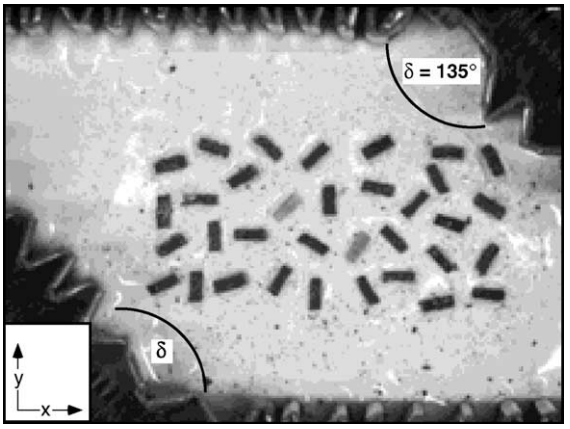

Fig. 1. Photograph of initial fabric of experiments and definition of the reference frame (x-, y-, z-direction) of the shear box; the x-axis is parallel to long sides of box, the y-axis is perpendicular to x and lies in the plane of the upper surface of sample. Observations are made in the xy-plane. δ is the initial angle between long and short sides of deformation box. Shown is the starting configuration of the object population with R_{ob}=3. Small particles of different color and size were randomly dispersed on the surface of the sample for flow analyses with the program PatMatch (Bons and Jessell, 1995).

1979; Tullis and Wood, 1975; Means et al., 1984; Willis, 1977).

Several parameters influence the development of the SPO of a population of rigid objects: object shape and aspect ratio, type of flow, finite strain, slip at the object/matrix interface, rheology of matrix material and density of the object population. The basis for understanding of the behaviour of a population of objects during progressive deformation is the knowledge of the behaviour of an individual isolated object in a deforming matrix. The influence of the aspect ratio of a rigid object on its rotation rate has been investigated using theoretical models based on the work of Jeffrey (1922). These models (e.g. Bhattacharyya, 1966; Gay, 1966, 1968; Rees, 1968, 1979; Reed and Tryggvason, 1974; Ghosh and Ramberg, 1976; Ferguson, 1979; Ježek et al., 1994) consider the rotation of an isolated axisymmetric ellipsoidal rigid object embedded in a deforming Newtonian viscous fluid. Individual rigid objects with an aspect ratio below some critical value, which depends on W_n, rotate cyclically in non-coaxial flow and, therefore, exhibit multiple revolutions during high straining. In a non-Newtonian matrix orbits of single ellipsoidal, nonspherical objects are not closed but drift towards a final position (Ferguson, 1979). Nevertheless, Jeffrey's model, which assumes a viscous Newtonian matrix material, is still likely to yield an acceptable approximation, except for very high strains (Ferguson, 1979). Analytical (e.g. Masuda et al., 1995), numerical (e.g. Pennacchioni et al., 2000) and experimental works (e.g. Ghosh and Ramberg, 1976; Odonne, 1994; Ildefonse et al., 1992b) have shown that in two-dimensional homogeneous flow, the rate of rota-

Table 1
Experimental conditions (PDMS=polydimethylsiloxane)

Type of deformation	Plane strain deformation
W_n	1, 0.8, 0.6
Initial dimensions [mm] ($x\times y\times z$)	150×100×100 mm
Initial angle, δ	135°
Finite simple shear strain of one experiment (two consecutive runs)	4.6 (W_n=1), 3.0 (W_n=0.8), 0.9 (W_n=0.6)
R_{xy} of one experiment (two consecutive runs)	22.7 (W_n=1), 13.1 (W_n=0.8), 2.6 (W_n=0.6)
Simple shear strain rate [s^{-1}] (W_n=1)	1×10^{-3} s^{-1}
Stretching rate along x-axis [s^{-1}] (W_n=0.8, 0.6)	3.3×10^{-4} s^{-1}
Matrix material ($\dot{\varepsilon}$=strain rate, σ=stress, η=viscosity, n=stress exponent)	(a) PDMS, linear Newtonian viscous, $\dot{\varepsilon}=(1/\eta)\sigma^n$; $\eta=3\times10^4$ Pa s; n=1 (b) PDMS+25% $BaSO_4$, nonlinear non-Newtonian viscous, power law behavior, $\dot{\varepsilon}\propto\sigma^n$; n=1.23
Object material	rigid India rubber
Object dimensions [mm]	6×2 mm, 5×2.5 mm
Density of object population [%] (area percentage of total area analysed)	14
Initial number of objects	34

tion of a rigid elliptical object in a Newtonian viscous fluid varies in a systematic manner depending on the kinematic vorticity, number of deformation (Means et al., 1980), the orientation of the long axis of the object, slip at the object/matrix interface and the aspect ratio of the inclusion.

The shape fabric evolution of a population of rigid neighbouring objects dispersed in a deforming matrix has been investigated experimentally (Fernandez, 1987; Ildefonse et al., 1992a,b; Ildefonse and Mancktelow, 1993; Albaret et al., 1996; Fernandez and Fernandez-Catuxo, 1997), numerically (e.g. Ježek et al., 1994, 1996) and analytically (e.g. Masuda et al., 1995). Experimental work has shown that mechanical interaction between rigid objects, perturbations of flow next to rigid objects and, therefore, the density of a population profoundly affects the developing fabric. It has been suggested that the angle β between the boundary of a shear zone and the mean resultant vector of all object orientations may under certain conditions closely correspond to the orientation α of the maximum finite stretching axis (e.g. Fernandez, 1987; Ildefonse et al., 1992a). This is the case at high aspect ratios (>10) and low-density rigid body population.

As analytical solutions for the influence of the mechanical interaction between rigid objects, perturbations of flow next to rigid objects and density of a population on the SPO are so far lacking; analytical and numerical works can only in parts be applied to SPOs seen in rocks. Due to experimental and mathematical restrictions, most analytical and experimental investigations usually consider only a Newtonian viscous matrix rheology and the two end-member deformation types: simple and pure shears. For example, experimental studies of the effect of particle interactions and density of object populations were exclusively performed for pure and for simple shears (e.g. Ildefonse et al., 1992a,b; Fernandez, 1987). Experiments using a power law matrix material were only done in simple shear (Ildefonse and Mancktelow, 1993).

In contrast to experimental and theoretical investigations, deforming rocks commonly follow power law flow (e.g. Carter, 1976; Schmid, 1976; Urai, 1983; Kirby and Kronenberg, 1987). In addition, deformation may deviate from simple and pure shears in a significant way (Passchier, 1987; Vissers, 1989; Masuda et al., 1995; Wallis, 1995; Beam and Fisher, 1999; Jiang, 1999). In this study, we present an investigation into the effect of different combinations of pure and simple shears, matrix rheology, object

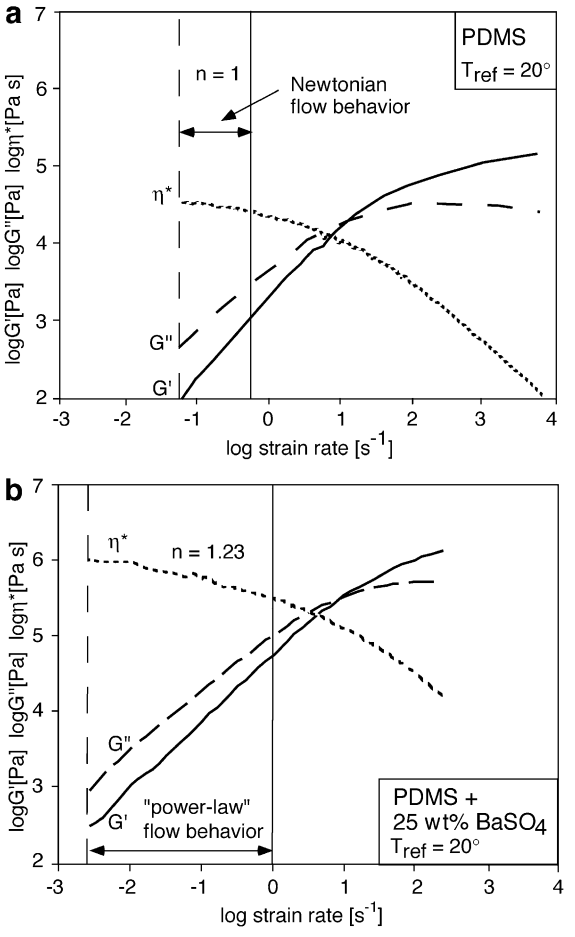

Fig. 2. Graphs of log strain rate against log storage modulus (G') and loss modulus (G''); different relations between G' and G'' signify different mechanical behaviour. Viscous behavior is characterised by $G'' \gg G'$. It is Newtonian if the slopes of G'' and G' are 1 and 2, respectively. η^* [Pa] is the complex viscosity. (a) Rheological data of polydimethylsiloxane (PDMS; Weijermars, 1986); plot showing G', G'' and η^* at a reference temperature (T_{ref}) of 20 °C, below a strain rate of 0.5 s^{-1}, PDMS shows viscous Newtonian flow behavior. (b) Rheological measurements of PDMS with 25 wt.% $BaSO_4$ show strain rate versus G', G'' and η^*. Below a strain rate of 16 s^{-1}, $G'' \gg G'$, indicating viscous flow behaviour. Below a strain rate of 1 s^{-1}, the slopes of G' and G'' have a constant value, indicating power law behavior with an power law exponent n=1.2 (ten Grotenhuis et al., 2002).

aspect ratio and resultant flow perturbation on the development of shape-preferred orientation of a population of rigid objects during progressive deformation.

2. Experimental set-up

Experiments were performed in a two-dimensional shear zone using a new apparatus with which it is possible to model homogeneous deformation in plane strain monoclinic regimes using a set-up of deformable pistons (Piazolo et al., 2001). In experiments, populations of 34 individual, rectangular objects made of India rubber were inserted with a random orientation in the deformation box (Fig. 1). The initial distance between two neighbouring objects was between 0.2 and 1.5 the length of its long axis. The density of the population of rigid objects is 14 area%. As a reference frame, we use orthogonal axes x, y and z where the surface of the shear box is the xy-plane, the longest side of the box lies parallel to the x-axis throughout the experiments, while the short side can rotate. The initial dimension of the shear box was $150\times100\times100$ mm and the angle δ between the long and short sides of the shear box was 135° at the beginning of each experiment (Fig. 1). Experiments were performed at a constant kinematic vorticity number W_n with no extension or shortening in the z-direction of the shear box. The shear sense was dextral in all experiments.

Three parameters were varied in experiments (Table 1): (1) aspect ratio R_{ob} (3 or 2) of individual rigid objects in the xy-plane (Fig. 1), (2) the kinematic vorticity number (1 (simple shear), 0.8 and 0.6) and (3) matrix material (PDMS or a mixture of PDMS and 25 wt.% $BaSO_4$). Polydimethylsiloxane (PDMS) is a Newtonian linear viscoelastic polymer. The rheology of the mixture used is non-Newtonian, nonlinear viscous with a power law exponent (n) of 1.2. The flow laws and the rheological properties of the used materials are given in Table 1 and Fig. 2, respectively. For more details, the reader is referred to ten Grotenhuis et al. (2002).

Experiments at W_n=1 were performed with a simple shear strain rate of 1×10^{-3} s^{-1}. In experiments with W_n=0.8 and W_n=0.6, the stretching rate along the x-axis was held constant at 3.3×10^{-4} s^{-1}. To achieve sufficiently high strain, it was necessary to perform two consecutive experimental runs. At the end of the first experimental run, the position and orientation of the objects was recorded and at the beginning of the second run each object was inserted with the recorded orientation and position. The cumulative finite simple

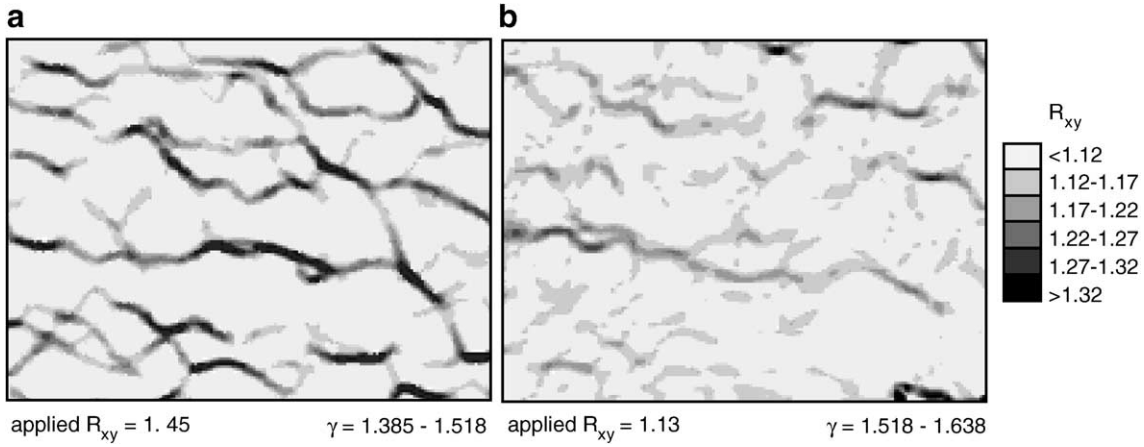

Fig. 3. Plots of R_{xy} in experiments with R_{ob}=3 for two strain intervals during progressive deformation at W_n=0.8 using the program PatMatch (Bons and Jessell, 1995). The matrix material has a power law flow behaviour (PDMS+25 wt.% $BaSO_4$). (a) Plot showing the geometry at the end of run 1 of the experiment; (b) plot showing the beginning of run 2. The position and orientation of high strain zones is similar in the two plots. This shows that the high strain zones develop rapidly and that at the beginning of the second experimental run high strain zones develop at similar position and orientation as seen at the end of the first run.

shear strain, which is the sum of the simple shear strain of the first and second experimental run, was 4.6 at W_n=1, 3.0 at W_n=0.8 and 0.9 at W_n=0.6. In terms of the axial ratios of the finite strain ellipse (R_{xy}), these values correspond to 22.7, 13.1 and 2.6, respectively (Table 1). An obvious problem of this set-up is that the spatial distribution of strain localization that develops in the matrix during the first run of the experiment is not present at the very beginning of the second run. In contrast to rocks, which change their rheological behaviour during deformation by for example grain size reduction or fracturing, the materials used do not significantly change their rheological behaviour with deformation. Therefore, the division of deformation in two runs should not effect the localization of deformation. To make sure that this assumption is true, we checked whether at the very beginning of the second run, similar patterns of strain localization developed as those observed at the end of the first run. Fig. 3 shows that this is the case.

3. Analytical methods

Analyses of experiments consisted of (1) measurement of the intensity of the SPO, (2) measurement of the mean orientation of the long axis of objects with respect to the *x*-direction of the shear zone, (3) comparison of the measured SPO intensity as a function of R_{xy}, W_n, finite strain and the corresponding analytically predicted SPO using the formulas provided by Ghosh and Ramberg (1976) and (4) investigation of flow characteristics.

The shape-preferred orientation of a fabric can be quantified using the statistical concentration parameter (κ) of a von Mises distribution (Masuda et al., 1999). The von Mises distribution is commonly referred to as the equivalent to a normal distribution that is specifically suitable to statistically evaluate orientation data. The concentration parameter κ is proportional to the normalized length (R) of the mean resultant vector of the oriented data, here the direction of the long axes of the objects. R ranges from 0 to 1 whereas κ ranges from 0 (no alignment) to infinity (perfect alignment). Using κ is preferred for its larger range of values. In our experiments, the accuracy at which κ can be determined is ± 0.15. In addition, the angle β of the mean orientation of the long axis of objects with respect to the *x*-direction of the shear zone is derived. This measured angle β can be determined with an accuracy of $\pm 3°$. β can then be compared to the corresponding theoretical angle α of the longest axis of the strain ellipse.

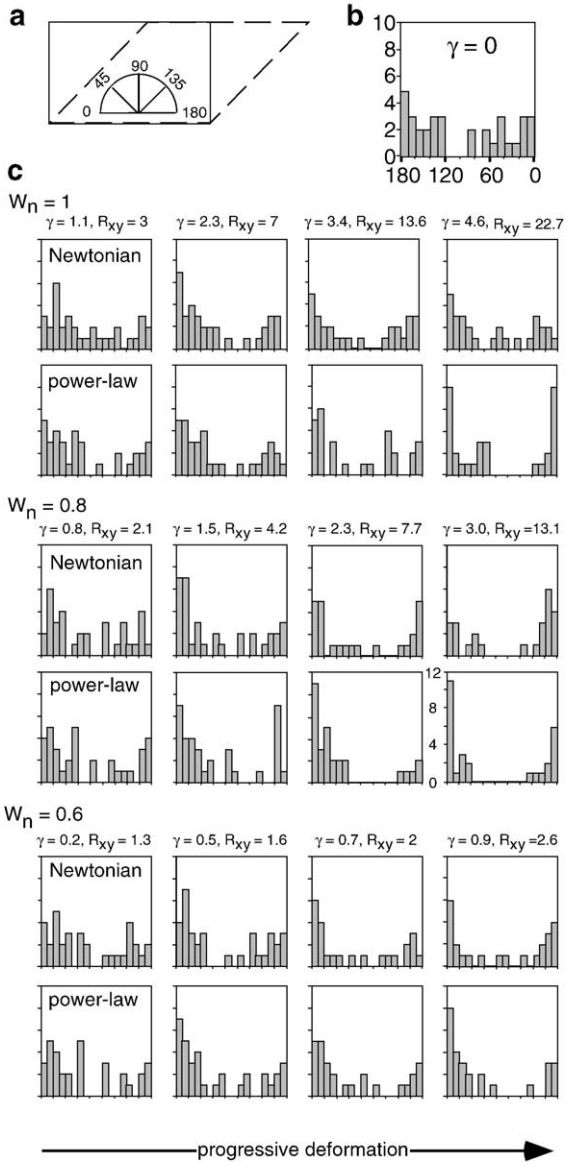

Fig. 4. Selected histograms of orientation of particles in experiments of R_{ob}=3. (a) Definition of the orientation of rigid objects; (b) initial orientations; (c) histograms.

The equations put forward by Ghosh and Ramberg (1976), which are used for comparison of theoretical values with experimental results, were derived for isolated, elliptical inclusions in a Newtonian viscous matrix, while in experiments objects are rectangular. However, these equations can be used here as rectangular objects rotate at approximately the same rate as elliptical objects with a similar axial ratio (ten Brink, 1996; Albaret et al., 2001).

The distribution of deformation within the samples was measured using the program PatMatch of Bons and Jessell (1995), which employs the pattern-matching method. This program measures the displacement field between two stages of deformation to derive various deformation parameters, such as the distribution of absolute finite strain (R_{xy}) and deformation of an imaginary initially perpendicular grid within a deformed sample. To determine the dominant orientation of high strain zones, the autocorrelation function (ACF) using NIH Image and the FFT macro (Rasband, 1996; Pannozzo Heilbronner, 1992) was applied to R_{xy} plots generated by PatMatch (Bons and Jessell, 1995). The ACFs were calculated for selected regions of interest of 512×512 pixels.

4. Experimental results

4.1. Rigid objects with aspect ratio R_{ob}=3

Four main characteristics of SPO are observed: (1) in all experiments, there is a pronounced discrepancy between analytically predicted and experimental κ values, particularly in experiments with power law matrix material and nonsimple shear deformation (Fig. 5a); (2) the intensity of SPO increases with decreasing W_n (Figs. 4 and 5a); (3) in a power law matrix material and in nonsimple shear experiments, κ is markedly higher than the analytically predicted values and higher than values observed within the Newtonian matrix (Figs. 4 and 5a); (4) angle β is always smaller than the corresponding angle α of the strain ellipse; and (5) in experiments with Newtonian matrix, the difference between β and α is largest and β can even become slightly negative (Fig. 6).

In experiments, SPO is not clearly periodic. For simple shear deformation, though, some periodicity may be expected to occur at higher strain than the applied strain because in theory objects with R_{ob}=3 rotate cyclically. Therefore, resultant SPOs should show some periodicity during high strain deformation. If, though, deformation is characterized by a significant pure shear component, objects should theoretically remain in a semi-stable position for long stretches of the deformation. Consequently, during further progressive deformation, SPO is not expected to decline significantly and develop a marked periodicity. Nevertheless, some fluctuations may still occur.

Significant strain localization during deformation was observed in all experiments (Fig. 7). Zones of relatively high R_{xy} in comparison to strain in the adjacent material anastomose and low strain zones develop close to the rigid objects. Trains of objects, bounded by shear zones, had a width of 1.2 to 1.6 times the longest axis of the rigid objects. Individual high strain zones remained stable for part of the progressive deformation history (Fig. 8). The geometry of anastomosing shear zones closely resembles the pattern of an anastomosing disjunctive foliation with cleavage domains and microlithons (e.g. Stephens et al., 1979). At W_n=1, high strain zones extend as continuous zones over most of the area analysed. High strain zones at an angle to the shear zone boundary are seen in all experiments with a variable degree of development. Application of the autocorrelation function (Pannozzo Heilbronner, 1992) to images depicting R_{xy} (cf. insets in Fig. 7) visualize the dominant orientation of the high strain zones. The angle ϕ between the boundary of the shear box (x-axis) and the dominant orientation of the high shear zones measured in a clockwise direction is similar

Fig. 5. Results of experiments plotting the intensity of shape preferred orientation (SPO) as a function of magnitude of the simple shear strain γ. Corresponding R_{xy} values are given at top of diagram. The intensity of SPO is given in values of the concentration parameter κ of a von Mises distribution. Depicted are measured κ values (measurement accuracy is $\pm$0.15; see error bar inset) and analytically predicted values (Ghosh and Ramberg, 1976). The results are reproducible to an accuracy of a κ value difference of 0.3. (a) Experiments with a population of objects with R_{ob}=3; (b) experiments with a population of objects with R_{ob}=2. Note that the κ value range differs significantly in (a) and (b).

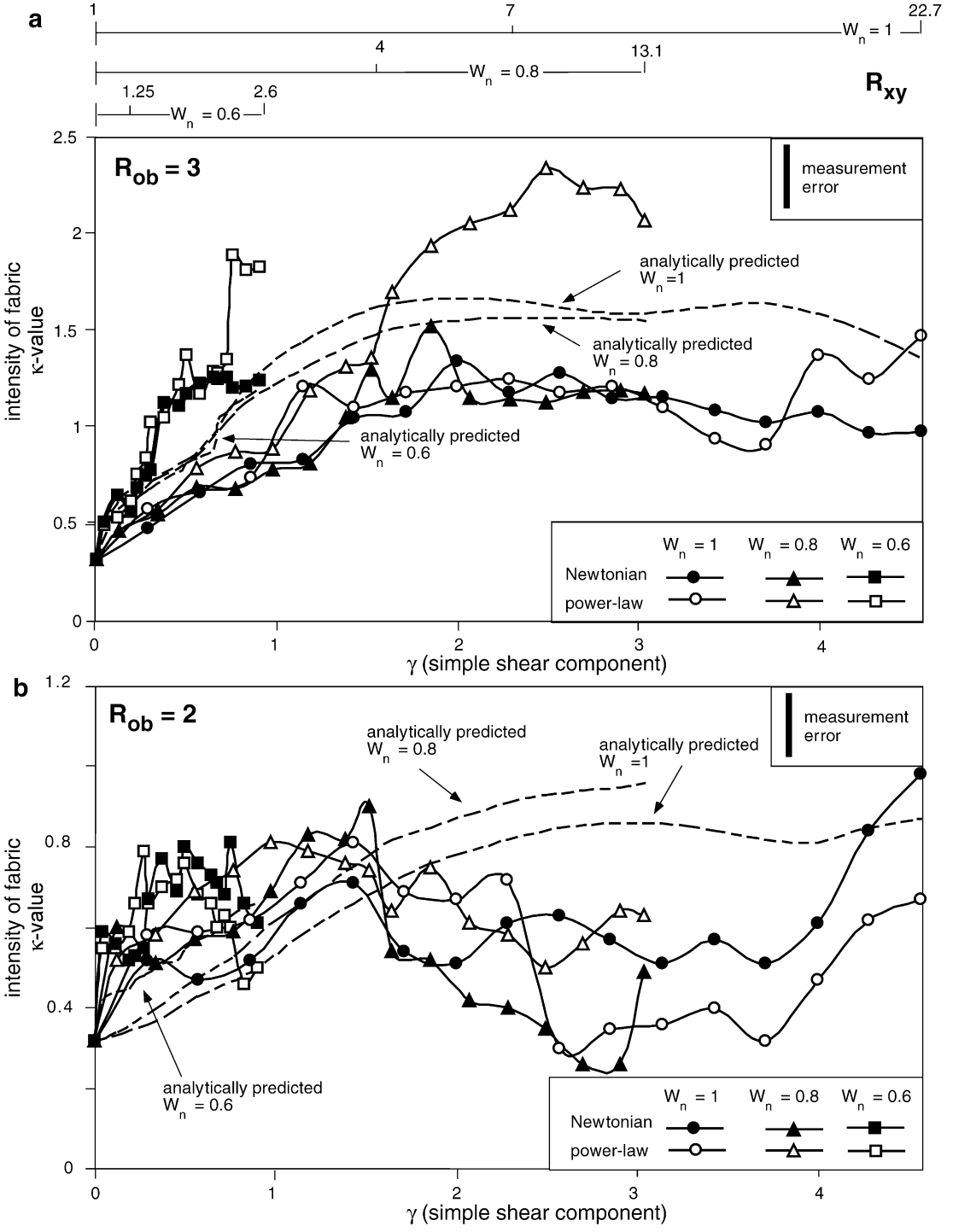
a
1
7
22.7
W_n = 1
4
13.1
W_n = 0.8
1.25
2.6
W_n = 0.6
R_xy
R_ob = 3
measurement error
analytically predicted W_n =1
analytically predicted W_n = 0.8
analytically predicted W_n = 0.6
W_n = 1
W_n = 0.8
W_n = 0.6
Newtonian
power-law
intensity of fabric κ-value
γ (simple shear component)
b
R_ob = 2
measurement error
analytically predicted W_n = 0.8
analytically predicted W_n =1
analytically predicted W_n = 0.6
W_n = 1
W_n = 0.8
W_n = 0.6
Newtonian
power-law
intensity of fabric κ-value
γ (simple shear component)

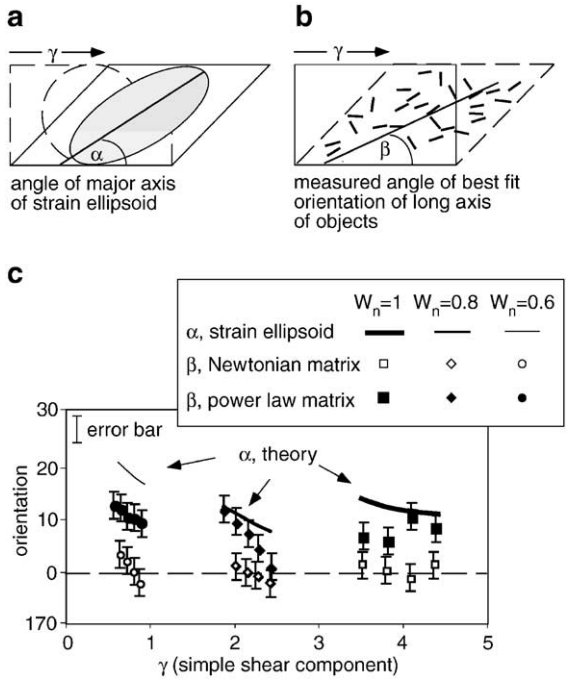

Fig. 6. Diagram illustrating the change in orientation of the mean orientation of a population of rigid objects with R_{ob}=3 during progressive deformation in comparison with orientation of the long axis of the strain ellipsoid. (a) α is the angle between the long axis of the strain ellipse and the x-axis. (b) β is the angle between the mean of the orientation of the objects and the x-axis. (c) Graph showing α and β as a function of the simple shear component of finite strain. The mean orientation of the objects can be determined with an accuracy of $\pm 3^\circ$ (see error bars).

within a range of 3–4° in experiments with the same type of deformation (W_n). It is 12° for W_n=0.6, 4° for W_n=0.8 and 176° for W_n=1. In other words, at W_n=0.6 and W_n=0.8, the orientation of the high strain zones is synthetic and at W_n=1 it is antithetic. The partitioning of deformation in high strain zones and low strain zones was calculated using the displacement of imaginary initially straight into deformed lines as shown in the deformed grid generated by PatMatch (cf. Fig. 7). The strain partitioning is significantly different in the two matrix materials but independent of W_n. In experiments with the Newtonian matrix material, 60–64% of the total deformation is accommodated by high strain shear zones; in the power law matrix material, the corresponding value is 70–76%.

In addition, deformed grids (Fig. 7b) show that strain partitioning is coupled with partitioning of pure (low strain zones) and simple shear components (high strain zones) during progressive deformation (Fig. 7b). Objects that lie parallel to the shear zone boundary are positioned in low strain, pure shear dominated zones and rotate different to predictions from theory. Over large stretches of the deformation, they remain nearly stable, although some rotation and back-rotation is observed. Objects that are initially at high angle to the flow plane rotate at a rotation rate similar to that predicted from theory (Ghosh and Ramberg, 1976) (Fig. 9).

4.2. Rigid objects with aspect ratio R_{ob}=2

Experiments using objects with an aspect ratio R_{ob}=2 (Fig. 5b) show (1) significantly lower SPO intensity than experiments with R_{ob}=3, (2) highly variable κ values throughout progressive deformation which seem to be periodic, (3) no systematic difference in SPO intensity at different W_n, (4) minor discrepancy between analytically predicted and experimental SPO intensity (in the range of its periodicity) and (5) no systematic difference in SPO with respect to matrix material properties.

Fig. 7. Flow analyses of experiments with objects of R_{ob}=3 for three different kinematic vorticity numbers W_n and two matrix materials. Long sides of the rectangular images are parallel to the x-axis of the deformation box (cf. Fig. 1). (a) Plots of R_{xy}. High strain zones appear as dark bands. Rectangular boxes show the position and orientation of objects as seen at the end of the deformation considered. In contrast to the shown position of the objects, the shown R_{xy} results from analyses of geometrical differences between two consecutive pictures taken at different stages of deformation. Therefore, some overlap of high strain zones and objects as represented now may occur. Dashed lines in legend represent the applied R_{xy}. In the experiments, high strain shear zones develop and separate trails of objects positioned in low strain areas. To the right of the diagrams, results from image analyses using the autocorrelation function (Pannozzo Heilbronner, 1992) are shown. These depict the dominant orientation of high strain zones. Note the change in angle with different vorticity. (b) Deformation of an imaginary, initially rectangular grid generated by the program PatMatch (Bons and Jessell, 1995). Figures correspond to diagrams shown in (a). In the deformed grid, simple shear zones appear dark due to tilt of grid lines. Pure shear zones show rectangles. White areas occur where the program had problems finding the corresponding pattern in the deformed sample. Such problems arise where light is reflected from the surface of the material.

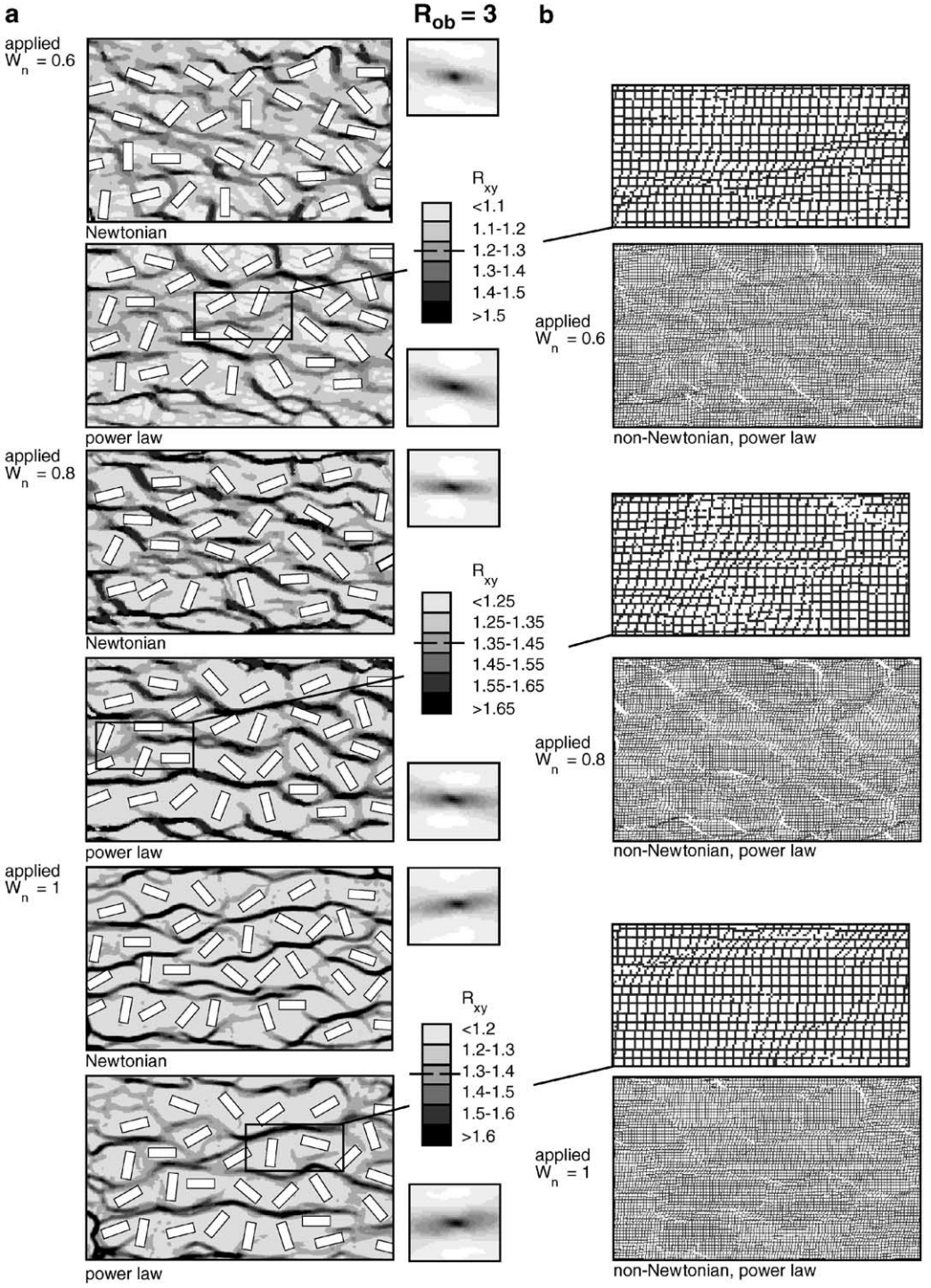
a
R_{ob} = 3
b
applied W_n = 0.6
Newtonian
power law
R_{xy}
<1.1
1.1-1.2
1.2-1.3
1.3-1.4
1.4-1.5
>1.5
applied W_n = 0.6
non-Newtonian, power law
applied W_n = 0.8
Newtonian
power law
R_{xy}
<1.25
1.25-1.35
1.35-1.45
1.45-1.55
1.55-1.65
>1.65
applied W_n = 0.8
non-Newtonian, power law
applied W_n = 1
Newtonian
power law
R_{xy}
<1.2
1.2-1.3
1.3-1.4
1.4-1.5
1.5-1.6
>1.6
applied W_n = 1
non-Newtonian, power law

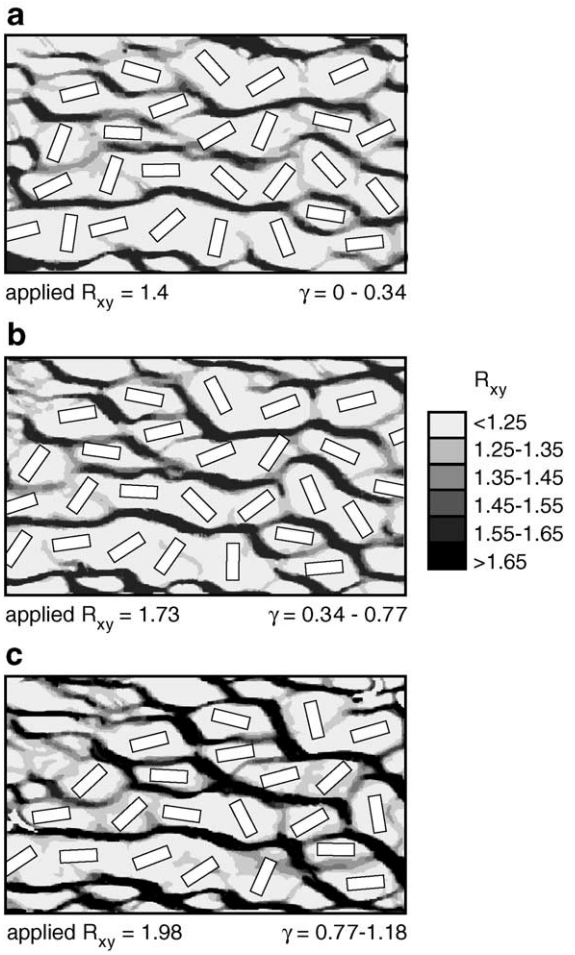

Fig. 8. Plots of R_{xy} in experiments with objects of R_{ob}=3 calculated from photographs taken at the beginning and end of three strain intervals during progressive deformation at W_n=0.8. The matrix material has a power law behaviour (PDMS+25 wt.% $BaSO_4$). Rectangular boxes show the position and orientation of objects at the end of the respective strain interval. Note that in contrast to the shown position of the objects. R_{xy} is shown results from analyses of geometrical differences between two consecutive pictures taken at different stages of deformation. Therefore, some overlap of high strain zones and objects as represented now may occur. (a) Simple shear strain γ=0–0.34, R_{xy}=1.4; (b) γ=0.34–0.77, R_{xy}=1.73; (c) γ=0.77–1.18, R_{xy}=1.98. During progressive deformation, the position of high strain shear zone remains largely constant.

As in experiments with R_{ob}=3, high strain zones are present in both matrix materials (Fig. 10). Low strain zones are seen close to rigid objects. At W_n=1, high strain zones extend over most of the analysed area (Fig. 10). The angle ϕ (for definition see above) is dependent on W_n, but independent of matrix material. The relationship between W_n and ϕ is very similar to that observed in experiments with R_{ob}=3 (13° for W_n=0.6, 2° for W_n=0.8 and 174° for W_n=1). Partitioning of W_n in simple shear and pure shear dominated zones is also observed in experiments with R_{ob}=2. The degree of partitioning is matrix-depend-

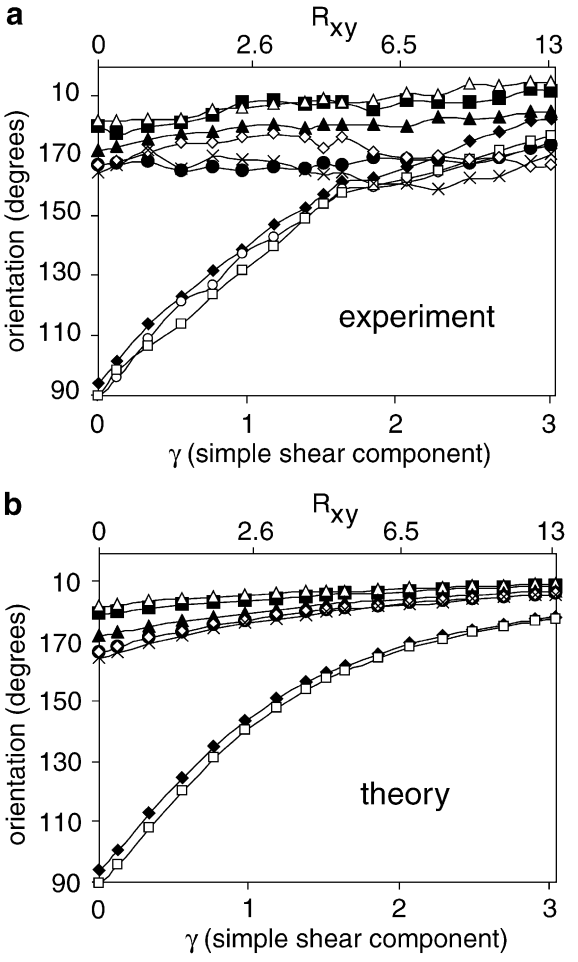

Fig. 9. (a) Graph showing the change in orientation of selected objects (R_{ob}=3) with increasing simple shear strain γ and R_{xy}. Note that the axial ratio R_{xy} increases nonlinearly with increasing simple shear strain γ. W_n is 0.8 and the matrix material has a power law behaviour (PDMS+25 wt.% $BaSO_4$); (b) corresponding change in orientation according to theory (Ghosh and Ramberg, 1976). In both graphs, the same symbols for the same objects are used. The definition of the angle of orientation is as shown in Fig. 4a. Note that in (b), no open circles are shown. In theory, the objects represented by this symbol exhibit the same change in orientation as the objects represented by open squares.

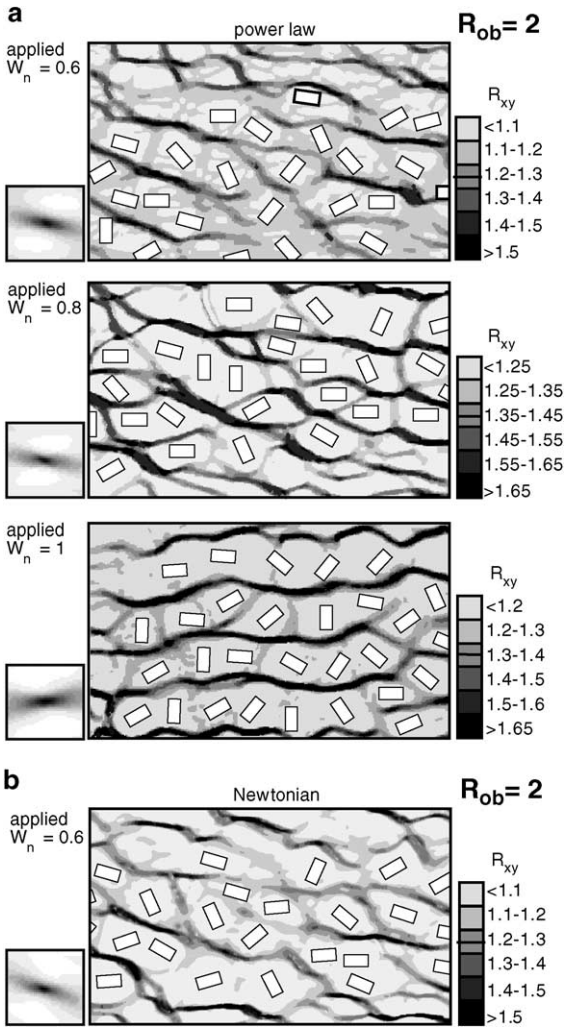

Fig. 10. Representation of the distribution of R_{xy} as calculated using PatMatch (Bons and Jessell, 1995) for experiments of rigid particles with R_{ob}=2 within the two different matrix materials. High strain zones appear dark and low strain zones light. Horizontal lines in legend represent the applied value of R_{xy} for the specific deformation type. Rectangular boxes show the position and orientation of objects. On the left of the R_{xy} plots results from image analyses using the autocorrelation function (Pannozzo Heilbronner, 1992) are shown. These depict the change in orientation of the dominant shear zone direction with a change in W_n. (a) Experiments with power law matrix material deformed at different W_n. (b) Experiment with Newtonian matrix material deformed at W_n=0.6.

ent; 70–73% and 60–62% of the deformations are accommodated in high strain zones in the power law material and Newtonian material, respectively. As shown in Fig. 5b, the SPO is low (0.3<κ value<1) and strongly variable throughout an experiment. Although in these experiments β can be determined, it is not meaningful in the sense of a reliable estimate for the mean orientation of a population of rigid objects. Therefore, it is not further considered here.

5. Discussion

5.1. Discussion of experimental results

From analytical studies of permanently rotating elongated objects in monoclinic non-coaxial flow with a set-up as realized in our experiments (e.g. Ghosh and Ramberg, 1976; Ježek et al., 1994, 1996; Masuda et al., 1995), it is known that their rotation rate is smallest when they are oriented with their long axis in the small angle between the flow eigenvectors in the *xy*-plane (minimum velocity position (MVP)). This minimum rotation rate decreases further with increasing aspect ratio and decreasing W_n. Accordingly, it is expected that high SPOs develop if elongated objects have a high aspect ratio and W_n is low.

Our experiments confirm these predictions: a high intensity of the SPO develops (1) in populations with aspect ratios of 3, and (2) at low W_n. Additionally, results show that for populations with an object ratio of 3, the intensity of SPO is higher in a power law matrix material than in Newtonian matrix material.

At high strain values in our experiments, the summed rotational behaviour of individual elongated objects of the object population with R_{ob}=3 results in a high shape-preferred orientation where the mean orientation of the longest axis of the objects develops at a small angle with the extensional flow eigenvector (*x*-axis in our experiments). In contrast, populations of objects with low aspect ratios (R_{ob}=2) produce low and periodically fluctuating SPO intensities (κ values) in all experiments. This finding confirms results of Pennacchioni et al. (2001), who state that SPOs developed in populations of R_{ob}<3 are low but of R_{ob}>3 (in our case, R_{ob}=3) are high.

In experiments, rigid objects lie in the pure shear dominated zones with low R_{xy} values and simple shear zones characterized by high R_{xy} value anastomose around objects. During progressive deformation, an object initially oriented at a high angle to the exten-

sional eigenvector is likely to be close to one of the high strain zones. Hence, it will rotate with a high rotation rate towards the MVP. An object that is oriented at a low angle to MVP is most likely to be positioned within a low strain, low W_n zone. Hence, its rotation rate will be slow and it will tend to remain with its long axis at a low angle to the MVP during progressive deformation. The partitioning of different rotation rates of objects that are oriented at high angle and low angle to the MVP is more pronounced for populations of high object aspect ratio than for those of low aspect ratios. Therefore, population of rigid objects of R_{ob}=3 remain at low angles to the shear zone boundary for a longer time than objects with lower aspect ratios. This results in high SPOs.

In all experiments with a power law matrix material, partitioning between high strain simple shear and low strain pure shear dominated zones is more pronounced than for a Newtonian matrix material. In a power law material, the high strain zones take up most of the deformation and are generally more discrete than in the Newtonian matrix material. The angle of the mean orientation of the high strain zones and the shear zone boundary depends on deformation type. At low W_n, the angle is synthetic and relatively large (12–14°), at medium W_n, it is synthetic and small (2–4°), and for simple shear (W_n=1), it is slightly inclined (4–6°) antithetically.

The observed flow partitioning resembles that proposed by Bell (1985, 1992), who suggested that non-coaxial deformation partitions into zones of nearly coaxial deformation and zones of generally non-coaxial shearing. Round porphyroblasts and porphyroclasts would lie within coaxial deformation zones and would rotate little or not at all with respect to bulk flow axes. In contrast to statements by Bell (1985, 1992), in our experiments, (a) rigid objects are elongated and (b) objects still rotate slightly during progressive deformation even if they are positioned in low strain zones. Further detailed studies are needed to evaluate the correspondence of suggestions by Bell (1985, 1992) and the experiments satisfactorily.

5.2. Geological application of experimental results

If flow in a material is partitioned, the pattern of strain and W_n partitioning has important implications for the development of (1) shape-preferred orientation of rigid object populations, (2) shear zones and (3) shear bands. It is also relevant for the applicability of flow type analyses in terms of kinematic vorticity number. The mean orientation of rigid objects can be used for shear sense determination for populations with R_{ob}=3 if the matrix material follows power law flow. It is limited if the matrix material is Newtonian. Quantitative strain analysis is to a limited extent possible for populations of R_{ob}=3. For populations with R_{ob}=2, the mean orientation of the objects can neither be used reliably for shear sense nor shear strain determination.

Intensities of SPO of rigid object populations in rocks are expected to be high if (1) the aspect ratios of the bodies (e.g. porphyroclast, porphyroblasts) are higher than 2; (2) the matrix material deforms by power law flow; and (3) deformation has a significant pure shear component. Localized shear zones extending over large areas are likely to develop in rocks characterized by power law rheology and competence heterogeneities. The spatial distribution of such shear zones will be strongly influenced by the rock rheology and major simple shear zones will develop at distance to the more rigid parts of the rock. The experiments suggest that the orientation of high strain zones with respect to the shear zone boundary could be used to determine the type of deformation in terms of kinematic vorticity number. Vorticity numbers smaller than 1 result in synthetic high strain zones, where the higher the component of pure shear deformation, the higher the angle ϕ and intensity of the high strain zones at an angle to the shear zone boundary. This observation supports the work of Passchier (1991), who proposed that so-called ECC-fabrics (extensional crenulation cleavage; Platt, 1979, 1984; White, 1979; Platt and Vissers, 1980) can develop more easily in stretching shear zones than shear zones with bulk simple shear flow. At simple shear, the mean orientation of high strain zones is slightly inclined antithetically.

Our experiments show that W_n may locally deviate significantly from the bulk applied W_n. Therefore, results from kinematic vorticity number analysis, which is performed in a localized volume of rock using for example porphyroclasts (Passchier, 1987; Vissers, 1989; Masuda et al., 1995; Wallis, 1995; Beam and Fisher, 1999), can only to a certain extent be extrapolated to the bulk deformation of the whole

rock. Especially in rocks in which the matrix exhibits power law rheology, locally derived kinematic vorticity numbers may be quite different from those of the bulk flow. This may even apply to Newtonian matrix materials. Measurements in several representative parts of such a fabric may give more accurate results for the bulk flow type.

The mean orientation of a population of rigid objects can be used as a shear sense indicator and estimate for shear strain in populations of R_{ob}=3 if the matrix material exhibits a power law flow behaviour. If the matrix is Newtonian, the observed mean orientation may be misleading and point to the wrong shear direction and evaluation of the shear strain is limited (cf. Fig. 6). For populations of R_{ob}=2, the mean orientation is not very well defined (low κ value) and its interpretation may lead to wrong shear sense determination as the orientation changes periodically. Due to the periodic change of the intensity of SPO, a meaningful estimation of shear strain is not possible.

When comparing and applying experimental results to real rocks, one has to be aware that rocks deforming in a ductile regime commonly exhibit a power law flow behaviour with a stress exponent between 2 and 5 (Kirby and Kronenberg, 1987). Hence, effects attributed to the nonlinearity of the rheology of the matrix material are expected to be more pronounced in nature than in experiments.

6. Conclusion

Analogue modelling of shape fabric development of a population of rigid objects dispersed in a viscous matrix shows that the shape-preferred orientation is a function of (1) aspect ratio of rigid objects, (2) the type of flow, (3) the rheological properties of the matrix material and (4) the accumulated strain.

Populations of object with an aspect ratio of 3 can be used for determination of shear sense and, to a limited extent, flow geometry, and for strain analysis. Analyses have to consider the significant influence of the rheology of the matrix material and particle interaction on the rotation rates of the rigid objects and development and intensity of SPO. Therefore, analysis will lead to qualitative but not necessary quantitative estimates. SPO of object populations with an aspect ratio of 2 or less are unreliable to determine shear sense and the intensity of shape-preferred orientation cannot be used to determine the finite strain.

The intensity of the developed SPO increases with an increase in the pure shear component of bulk flow. In a matrix material with power law flow behaviour, the intensity of the shape-preferred orientation is higher than in a Newtonian material. In both matrix materials, high strain simple shear zones develop. Adjacent are low strain pure shear dominated zones, which are characterized by relatively stable similarly orientated trains of rigid objects oriented at low angles to the extensional eigenvector or shear plane. Partitioning between high strain simple shear and low strain pure shear dominated flow is most pronounced in the power law material. Therefore, in such materials, kinematic vorticity analyses on the scale of partitioning may not necessarily represent the kinematic vorticity of bulk flow.

Acknowledgements

SP acknowledges the financial support of the German Research Foundation (GRK 392/1). Special thanks to Ralf Halama (University of Mainz) and Birte Anders (University of Mainz) for their assistance during experiments and analyses. Constructive comments by T. Horscroft, G. Pennacchioni and an anonymous reviewer improved the manuscript considerably and are hereby gratefully acknowledged.

References

Albaret, L., Diot, H., Bouchéz, J.L., 1996. Shape fabrics of particles in low concentration suspensions: 2D analogue experiments and application to tiling in magma. Journal of Structural Geology 18, 941–950.

Albaret, L., Mancktelow, N.S., Burg, J.-P., 2001. Effect of shape and orientation on rigid particle rotation and matrix deformation in simple shear flow. Journal of Structural Geology 23, 113–125.

Beam, E.C., Fisher, D.M., 1999. An estimate of kinematic vorticity from rotated elongate porphyroblasts. Journal of Structural Geology 21, 1553–1559.

Bell, T.H., 1985. Deformation partitioning and porphyroblast rotation in metamorphic rocks: a radical reinterpretation. Journal of Metamorphic Geology 3, 109–118.

Bell, T.H., 1992. Porphyroblast inclusion-trail orientation data: eppure non son girate! Journal of Metamorphic Geology 10, 295–307.

Bhattacharyya, D.S., 1966. Orientation of mineral lineation along the flow direction in rocks. Tectonophysics 3, 29–33.

Bons, P.D., Jessell, M.W., 1995. Strain analysis in deformation experiments with pattern matching or a stereoscope. Journal of Structural Geology 17, 917–921.

Bouchéz, J.L., 1997. Granite is never isotropic: an introduction to AMS studies of granitic rocks. In: Bouchéz, J.L., Hutton, D.H.W., Stephens, W.E. (Eds.), Granite: From Segregation of Melt to Emplacement Fabrics. Kluwer Academic Publishers, Dordrecht, pp. 95–112.

Carter, N.L., 1976. Steady state flow of rocks. Reviews of Geophysics and Space Physics 14, 301–360.

Ferguson, C.C., 1979. Rotations of elongate rigid particles in slow non-Newtonian flows. Tectonophysics 60, 247–262.

Fernandez, A., 1987. Preferred orientation developed by rigid markers in two-dimensional simple shear strain: a theoretical and experimental study. Tectonophysics 136, 151–158.

Fernandez, A., Fernandez-Catuxo, J., 1997. 3D biotite shape fabric experiments under simple shear strain. In: Bouchéz, J.L., Hutton, D.H.W., Stephens, W.E. (Eds.), Granite: From Segregation of Melt to Emplacement Fabrics. Kluwer Academic Publishers, Dordrecht, pp. 145–157.

Gay, N.C., 1966. Orientation of mineral lineation along the flow direction in rocks: a discussion. Tectonophysics 3, 559–564.

Gay, N.C., 1968. Pure shear and simple shear deformation of inhomogeneous viscous fluids: 1. Theory. Tectonophysics 5, 211–234.

Ghosh, S.K., Ramberg, H., 1976. Reorientation of inclusions by combination of pure shear and simple shear. Tectonophysics 34, 1–70.

Ildefonse, B., Mancktelow, N., 1993. Deformation around rigid particles: the influence of slip at the particle/matrix interface. Tectonophysics 221, 345–359.

Ildefonse, B., Lardeaux, J.-M., Caron, J.-M., 1990. The behaviour of shape preferred orientation in metamorphic rocks: amphiboles and jadeites from the Monte Mucrone area (Sesia–Lanzo zone, Italian Western Alps). Journal of Structural Geology 12, 1005–1011.

Ildefonse, B., Launeau, P., Bouchéz, J.-L., Fernandez, A., 1992a. Effect of mechanical interactions on the development of shape preferred orientations: a two-dimensional experimental approach. Journal of Structural Geology 14, 73–83.

Ildefonse, B., Sokoutis, D., Mancktelow, N., 1992b. Mechanical interactions between rigid particles in a deforming ductile matrix. Analogue experiments in simple shear flow. Journal of Structural Geology 14, 1253–1266.

Jeffrey, G.B., 1922. The motion of ellipsoidal particles in a viscous fluid. Proceedings of the Royal Society of London 102, 161–179.

Ježek, J., Melka, R., Schulmann, K., Venera, Z., 1994. The behaviour of rigid triaxial ellipsoidal particles in viscous flows—modeling of fabric evolution in a multiparticle system. Tectonophysics 229, 165–180.

Ježek, J., Schulmann, K., Segeth, K., 1996. Fabric evolution of rigid inclusions during mixed coaxial and simple shear flows. Tectonophysics 257, 203–221.

Jiang, D., 1999. Vorticity decomposition and its application to sectional flow characterization. Tectonophysics 301, 243–259.

Kirby, S.H., Kronenberg, A.K., 1987. Rheology of the lithosphere: selected topics. Reviews of Geophysics 25, 1219–1244.

Masuda, T., Michibayashi, K., Ohta, H., 1995. Shape preferred orientation of rigid particles in a viscous matrix: re-evaluation to determine kinematic parameters of ductile deformation. Journal of Structural Geology 17, 115–129.

Masuda, T., Kugimiya, Y., Aoshima, I., Hara, Y., Ikei, H., 1999. A statistical approach to determination of mineral lineation. Journal of Structural Geology 21, 467–472.

Means, W.D., Hobbs, B.E., Lister, G.S., Williams, P.F., 1980. Vorticity and non-coaxiality in progressive deformation. Journal of Structural Geology 2, 371–378.

Means, W.D., Williams, P.F., Hobbs, B.E., 1984. Incremental deformation and fabric development in a KCl–mica mixture. Journal of Structural Geology 6, 391–398.

Odonne, F., 1994. Kinematic behaviour of an interface and competence contrast: analogue models with different degrees of bonding between deformable inclusions and their matrix. Journal of Structural Geology 16, 997–1006.

Pannozzo Heilbronner, R., 1992. The autocorrelation function: an image processing tool for fabric analysis. Tectonophysics 212, 351–370.

Passchier, C.W., 1987. Stable positions of rigid objects in non-coaxial flow—a study in vorticity analysis. Journal of Structural Geology 9, 679–690.

Passchier, C.W., 1991. Geometric constraints on the development of shear bands in rocks. Geologie en Mijnbouw 30, 203–211.

Pennacchioni, G., Fasolo, L., Cecchi, M.M., Salasnich, L., 2000. Finite-element modelling of simple shear flow in Newtonian and non-Newtonian fluid around a circular rigid particle. Journal of Structural Geology 22, 683–692.

Pennacchioni, G., Di Toro, G., Mancktelow, N.S., 2001. Strain-insensitive preferred orientation of porphyroclasts in Monte Mary myonite. Journal of Structural Geology 23, 1281–1298.

Piazolo, S., ten Grotenhuis, S.M., Passchier, C.W., 2001. A new apparatus for controlled general flow modelling of analogue material. Society of the American Geological Memoir 193, 249–258.

Platt, J.P., 1979. Extensional crenulation cleavage. Journal of Structural Geology 1, 95–96.

Platt, J.P., 1984. Secondary cleavages in ductile shear zones. Journal of Structural Geology 6, 439–442.

Platt, J.P., Vissers, R.I.M., 1980. Extensional structures in anisotropic rocks. Journal of Structural Geology 2, 397–410.

Rasband, W., 1996. NIH Image. National Institute of Health, Research Services Branch NIMH.

Reed, L.J., Tryggvason, E., 1974. Preferred orientation of rigid particles in a viscous matrix deformed by pure shear and simple shear. Tectonophysics 24, 85–98.

Rees, A.I., 1968. The production of preferred orientation in a concentrated dispersion of elongated and flattened grains. Journal of Geology 76, 457–465.

Rees, A.I., 1979. The orientation of grains in a sheared dispersion. Tectonophysics 58, 275–287.

Schmid, S.M., 1976. Rheological evidence for changes in the deformation mechanism of Solenhofen limestone towards low stresses. Tectonophysics 31, T21–T28.

Stephens, M.B., Glasson, M.J., Keays, R.R., 1979. Structural and chemical aspects of metamorphic layering development in metasediments from Clunes, Australia. American Journal of Science 29, 129–160.

ten Brink, C.E., 1996. Development of porphyroclast geometry during non-coaxial flow. Geologica Ultraiectina 142, 163 pp.

ten Grotenhuis, S.M., Piazolo, S., Pakula, T., Passchier, C.W., Bons, P.D., 2002. Are polymers suitable rock-analogs? Tectonophysics 350, 35–47.

Tullis, T.E., Wood, D.S., 1975. Correlation of finite strain from both reduction bodies and preferred orientation of mica in slate from Wales. Bulletin of the Geological Society of America 86, 632–638.

Urai, J.L., 1983. Deformation of wet salt rocks. PhD Thesis, Utrecht University, pp. 1–223.

Vernon, R.H., 2000. Review of microstructural evidence of magmatic and solid-state flow. Electronic Geosciences 5, 2.

Vissers, R.L.M., 1989. Asymmetric quartz *c*-axis fabric and flow vorticity: a study using rotated garnet. Journal of Structural Geology 11, 231–244.

Wallis, S., 1995. Voticity analysis and recognition of ductile extension in the Sanbagawa belt, SW Japan. Journal of Structural Geology 17, 1077–1093.

Weijermars, R., 1986. Flow behaviour and physical chemistry of bounding putties and related polymers in view of tectonic laboratory applications. Tectonophysics 124, 325–358.

White, S.H., 1979. Large strain deformation: report on a Tectonic Studies Group discussion meeting held at Imperial College London. Journal of Structural Geology 1, 333–339.

Willis, D.G., 1977. A kinematic model of preferred orientation. Bulletin of the Geological Society of America 88, 883–894.